Pak. j. sci. ind. res. Ser. A: phys. sci. 2024 **67A**(3) 251-260

Heat Transfer in Mixed Convective Flow of Magnetic-Ferrofluid Over a Stretching Porous Disk with Variable Thickness

Islam Zari[a]*, Rukhsana Parveen[a], Fatima Ali[a], Tahir Saeed Khan[a] and Fahim Ullah[b]
[a]Department of Mathematics, University of Peshawar, Khyber Pakhtunkhwa-25000, Pakistan
[b]University of Science and Technology Bannu, Khybar Pakhtunkhwa-28100, Pakistan.

(received September 29, 2021; revised February 1st, 2023; accepted April 10, 2023)

Abstract. This presentation highlights the heat transfer analysis in the mixed convective ferrofluid flow with variable thickness in numerous directions towards a rotating stretching disk. The magnetic field and porous medium are taken into consideration within the flow model, which has a plethora of packages in science, engineering and production zones. The equation of energy is scrutinized with the impact of nonlinear radiative terms. Convergent solution of the transformed system is simulated *via* the analytical procedure homotopy analysis method (HAM) with the help of MATHEMATICA software. It is noticed that for a higher amount of stretching parameter and disk thickness, the radial and axial velocities are enhanced. For higher values of radiation parameter, the Nusselt number increases, while it is decreased for larger value of power index law of disk thickness. Graphs of Nusselt number (heat transfer rate), Skin friction, temperature and velocity profiles are illustrated for the physical presentation of distinct fluid flow parameters.

Keywords: mixed convection, ferrofluid, magnetic field, rotating disk, thermal radiation, porous medium, variable thickness

Introduction

The heat transfer rate is one of the principal technologies of fluid mechanics which has a dominant role in wonderful zones of commercial and industrial networks (Khan *et al*., 2021; Gul *et al*., 2020a,b,c). In this context, ferrofluid is more wonderful for heat transfer enhancement as compared with the conventional nanofluids (non-magnetic nanofluids). Ferrofluid is a type of liquid that is attracted by the poles of a magnet. It is the colloidal compound where magnetic nanoparticles such as $CoFe_2O_4$, Fe_3O_4 (magnetite) and $NiFe_2O_4$ are separated by owing fluid and an organic compound. In 1962 O'Conor made ferrofluids and they were classified by Stephen Papal in 1965. They considered the ferrofluids for the magnetic field to change the flow structure. Due to its magnetic properties, interesting applications can be seen especially in medical and industrial zones such as separation of material, sensors solar cells, cooling speaker treatment of cancer, liquid micro robots and bee cavity (Huang *et al*., 2021; Zontul *et al*., 2021; Bhandari *et al*., 2020). The thermal performance highlighted by Sadeghi *et al*. (2021) in ferrofluid-filled wavy enclosures with magnetic fields. They represented the flow with two cylinders. Dhibi and Ben (2021) executed the numerical simulation of ferrofluid convective flow in the cubical enclosure. They examined the effect of a magnetic field over an inner spherical hot block. Salawu *et al*. (2021) numerically examined the impact of magnet, variable viscosity and conductivity on Von Karman swirling flow of ferromagnetic nanoliquids from a spinning disk. Socoliuc and Marin (2021) investigated the impact of long time exposure to light of ferrofluid on its low complex magnetic permeability. Shamshuddin and Eid (2021) explored the magnetic nanoliquid flow of ferromagnetic based nanoparticles from parallel rotating disk with viscosity and conductivity.

For the last few decades, flow around rotating surfaces has been a very famous region of research. It is due to its relevance in engineering and industrial sectors inclusive of jet vehicles, meals processing, electric power generating machine and turbine machine, ship propellers, pumps, jet engines, vacuum cleaners and flows in turbomachinery and cosmology (Mongia *et al*., 2022; Salawu *et al*., 2022; Shamshuddin *et al*., 2021). Nowadays, regular use of disks containing variable thickness is more demanding, due to its economic considerations and to enhance the mechanical performance of many industrial machines. Zari *et al*. (2022) theoretically analyzed the Hiemenz flow over a Riga surface in hybrid nanoliquid. Agarwal and

*Author for correspondence; E-mail: zari145@yahoo.com

Chakraborty (2022) elaborated the Ree-Eyring fluid due to rotated disks with radiation impact. Sharma *et al*. (2022) numerically simulated the MHD convective flow towards rotating disks with different effects. Shahzad *et al*. (2022) studied the second order convergence for Hall effect and Lorentz force on ternary nanofluid flowing by rotating disk. Some other interesting work related to rotating disks can be seen in literature (Shahzad *et al*., 2022; Shamshuddin *et al*., 2022; Shamshuddin *et al*., 2019).

In fluid mechanics problems, fluid flow in porous media is the way in which fluids behave whilst flowing *via* a porous medium, for instance sponge or wooden, or while filtering water the usage of sand or another porous material. As typically discovered, a few fluid flows through the media, while a few mass of the fluid is saved within the pores gift within the media. Porous materials based filling of cavities is a good achievement of the thermal process. In this regard, Algehyne *et al*. (2022) executed the Darcy-Forchheimer flow with the energy/mass transfer through a permeable plate. Haq *et al*. (2020) highlighted a fractional viscous fluid with impacts of MHD over a porous surface. The results declared that the downward trend is to be noted in a fluid motion for the increased amount of effective permeability number. Gul *et al*. (2020a,b,c) executed the study of controlling the melting process by porous medium and magnetic field. They observed that the aid of the porosity in the flow system can be utilized as a controlling agent for the removed melt and to preserve the thin layer melt thickness.

Previously, researchers have been given much attention to flow around a rotating disk with negligible thickness into various directions. In fact, it is difficult to find a study related to radiation. Further, the radiation based flow by stretching a rotating disk having variable thickness into various directions is not studied yet. The novelty of this research works to fill this void. The effect of MHD is also included in the model. The proposed problem is further simulated through a well-known analytical procedure HAM (Prusty *et al*., 2021; Saratha *et al*., 2021; Zari *et al*., 2021).

Considering steady 3D magneto mixed convective flow of ferrofluid flow. Proposed flow is formulated by assuming stretching rate c and angular velocity Ω due to stretching and rotating disk. The surface is expressed as:

$z=a((r/R_0)+1)^{\zeta}$

and in presence of variable thickness fluid absorbs the semi-infinite region over the disk. We assumed T_w is disk temperature and T_∞ is temperature far away from disk. The magnetic field of strength B_0 is applied, which is parallel to the z-axis. The Hartmann number is the ratio of electromagnetic force to the viscous force and it is frequently encountered in fluid flows through magnetic fields. Therefore, M is considered as a Hartmann number which has a magnetic field B_0. The physical sketch can be seen in Fig. 1. Using the above flow assumptions, mathematical equations can be represented as (Sadeghi *et al*., 2021; Bhandari *et al*., 2020).

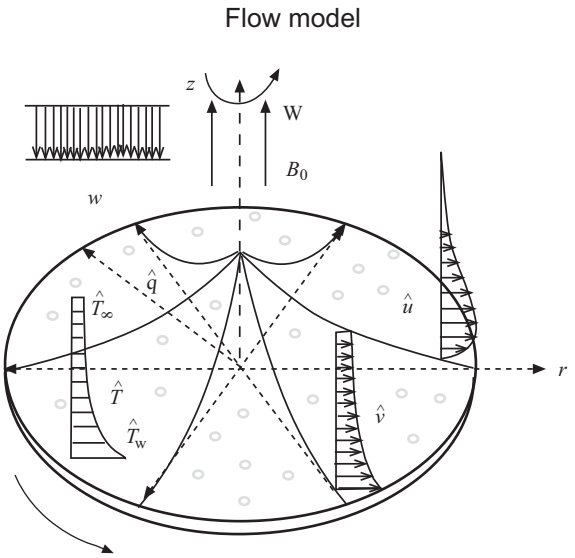

Fig. 1. Physical appearance of the flow model.

$$\frac{\partial \breve{u}}{\partial \breve{r}} = -\frac{\partial \breve{w}}{\partial \breve{z}} - \frac{\breve{\mu}}{\breve{r}} \quad \text{.....(1)}$$

$$\breve{u}\left(\frac{\partial \breve{u}}{\partial \breve{r}}\right) = \frac{\breve{v}^2}{\breve{r}} + \nu\left(\frac{\partial^2 \breve{u}}{\partial \breve{z}^2}\right) - \frac{\sigma}{\rho}(B_0^2 \breve{u}) - \left(\frac{\nu}{k}\right)\breve{u} + g_0 B_T (T - T_\infty) - \breve{w}\frac{\partial \breve{u}}{\partial \breve{z}} \quad \text{.....(2)}$$

$$-\frac{\breve{u}\breve{v}}{\breve{r}} = \breve{u}\frac{\partial \breve{v}}{\partial \breve{r}} + \nu\frac{\partial^2 \breve{v}}{\partial \breve{z}^2} - \frac{\sigma}{\rho}B_0^2 \breve{v} - \frac{\nu}{k}\breve{v} - \breve{w}\frac{\partial \breve{u}}{\partial \breve{z}} \quad \text{.....(3)}$$

$$\frac{1}{(\rho c_p)_f}\frac{\partial T}{\partial \breve{r}} - \breve{w}\frac{\partial T}{\partial \breve{z}} + \frac{\partial^2 T}{\partial \breve{z}^2} = \sigma B_0^2(\breve{u}^2 + \breve{v}^2) + \left(k + \frac{16\sigma^* T_\infty^3}{3k^*}\right), \quad \text{..(4)}$$

with

$$T = T_{\breve{w}},\ \breve{w} = 0,\ \breve{v} = \Omega\breve{r},\ \breve{u} = c\breve{r},\ \text{for}\ \breve{z} = a(\tau + 1)^{-\zeta},$$
$$T = T_\infty,\ \breve{w} = 0,\ \breve{v} = 0,\ \breve{u} = 0,\ \text{for}\ \breve{z} \to \infty \quad \text{.....(5)}$$

Here, (u, v, w) are components of velocity, B_0 is conduction, k^* is showing mean absorption, k is thermal conductive term of fluid, b is thickness coefficient and to be considered very small, R_0 signifies the feature radius, B_T is thickness index of the surface. The general form of Von Karman similarity transformations are (Bhandari *et al*., 2020)

$$\theta = \frac{T - T_\infty}{T_{\breve{w}} - T_\infty},\ \xi = \frac{\breve{z}}{R_0}(1+\tau)^{\varsigma}\left(\frac{\Omega R_0^{\,2}\rho}{\mu}\right)^{\frac{1}{n+1}} \quad \text{.....(6)}$$

Eq. (1) is axiomatically satisfied whereas, Eqs. (2)-(5) after substituting Eq. (6) can be reserved as follows:

$$2\breve{F}+\breve{H}'+\xi\grave{o}\zeta\breve{F}' = 0, \quad \text{.....(7)}$$

$$\breve{F}''(Re)^{\frac{1-n}{1+n}}(1+\tau)^{2\varsigma} - \breve{F}^2 + \breve{G}^2 - \xi\grave{o}\zeta\breve{F}\breve{F}' - \breve{H}\breve{F}' - M\breve{F} - \beta\breve{F} + Gr\vartheta = 0 \quad \text{.....(8)}$$

$$\breve{G}''(Re)^{\frac{1-n}{1+n}}(1+\tau)^{2\varsigma} - 2\breve{F}\breve{G} - \breve{H}\breve{G}' - M\breve{G} - \beta\breve{G} - \xi\grave{o}\zeta\breve{F}\breve{G}' = 0 \quad \text{.....(9)}$$

$$\frac{1}{Pr}(1+R)(Re)^{\frac{1-n}{1+n}}\vartheta'' + M\psi\breve{F}^2 + M\psi\breve{G}^2 - \xi\grave{o}\zeta\breve{F}\vartheta' - \breve{H}\vartheta' = 0 \quad \text{.....(10)}$$

$$\vartheta(\infty) = 0,\ \vartheta(\alpha) = 1,\ \breve{G}(\infty) = 0,\ \breve{G}(\alpha) = 1,\ \breve{F}(\infty) = 0,\ \breve{F}(\alpha) = A,\ \breve{H}(\infty) = 0 \quad \text{.....(11)}$$

Here, ò is the dimensionless constant, ς is the disk thickness, τ is the dimensionless radius, M is the Hartmann number, Re is the Reynolds number, Pr is Prandtl number, β is the porous parameter, ψ is the Eckert number, A is the scaled stretching parameter, and R is the radiation parameter, respectively.

$$\beta = \frac{\nu}{k\Omega},\quad M = \frac{\sigma}{\rho\Omega}B_0^2,\quad R = \frac{16\sigma^3 T_\infty^3}{3KK^*},\quad \Pr = \frac{\rho c_{pf}\nu}{k},$$

$$Re = \frac{\Omega R_0^2\rho}{\mu},\ A = \frac{c}{\Omega},\ \tau = \frac{1}{R_0},\ Ec = \psi = \frac{\rho\Omega^2}{(\rho c_{pf})(T_w - T_\infty)},$$

$$Gr = \frac{g_0 B_T(T_w - T_\infty)}{\Omega^2},\ \grave{o} = \frac{\tau}{R_0+\tau} \quad \text{.....(12)}$$

We introduced the deformations as

$$\theta = \theta(\xi-\alpha) = \theta(\xi),\ \breve{G} = \breve{g}(\xi-\alpha) = \breve{g}(\xi),\ \breve{H} = \breve{h}(\xi-\alpha) = \breve{h}(\xi),\ \breve{F} = \breve{f}\,(\xi-\alpha) = \breve{f}\,(\xi) \quad \text{.....(13)}$$

Eqs. (7)-(11) can be reduce into the forms are

$$\xi\grave{o}\zeta\breve{f}' = -\breve{h}' - 2\breve{f} \quad \text{.....(14)}$$

$$-\breve{f}^2 + \breve{g}^2 - (\xi+\alpha)\grave{o}\zeta\breve{f}\breve{f}' - \breve{h}\breve{f}' - M\breve{f} - \beta\breve{f} + Gr\theta = \breve{f}''(Re)^{\frac{1-n}{1+n}}(1+\tau)^{2\varsigma} \quad \text{.....(15)}$$

$$\breve{g}''(Re)^{\frac{1-n}{1+n}}(1+\tau)^{2\varsigma} - 2\breve{f}\,\breve{g} - \breve{h}\breve{g} - \beta\breve{g} = M\breve{g} + (\xi+\alpha)\grave{o}\zeta\breve{f}\,\breve{g}' \quad \text{.....(16)}$$

$$\frac{1}{Pr}(1+R)(Re)^{\frac{1-n}{1+n}}\theta'' + M\psi\breve{f}^2 + M\psi\breve{g}^2 - (\xi+\alpha)\grave{o}\zeta\breve{f}\theta' - \breve{h}\theta' = 0 \quad \text{.....(17)}$$

$$\theta(\infty) = 0,\ \theta(\alpha) = 1,\ \breve{g}(\infty) = 0,\ \breve{g}(\alpha) = 1,\ \breve{f}\,(\infty) = 0,\ \breve{f}\,(\alpha) = A,\ \breve{h}(\infty) = 0 \quad \text{.....(18)}$$

Here, h', f' are radial, tangential and axial velocities, respectively. However, θ' its temperature profile. The radial and tangential shear stresses at the lower disk are (Sadeghi *et al*., 2021)

$$s_{zr} = \mu\left(\frac{\partial\breve{u}}{\partial\breve{r}}\right)\Big|_{\breve{z}=0} = \mu\tau\Omega_1 R_0(1+\tau)^{\varsigma}\left(\frac{\Omega R_0^2\rho}{\mu}\right)^{\frac{1}{n+1}}\breve{f}\,'(0),$$

$$s_{\breve{z}\theta} = \mu\left(\frac{\partial\breve{v}}{\partial\breve{r}}\right)\Big|_{\breve{z}=0} = \mu\tau\Omega_1 R_0(1+\tau)^{\varsigma}\left(\frac{\Omega R_0^2\rho}{\mu}\right)^{\frac{1}{n+1}}\breve{g}'(0) \quad \text{..(19)}$$

The total shear stress s_w can be written as (Sadeghi *et al*., 2021)

$$s_w = \sqrt{s_{zr}^2 + s_{z\theta}^2} \quad \text{.....(20)}$$

skin friction coeffient $C_{f\breve{z}}$ is

$$C_{f\breve{z}}(Re)^{\frac{n-1}{n+1}} = \frac{(\breve{s}_w)|_{z=0}}{\rho(\breve{r}\Omega)^2}\frac{1}{\tau}(1+\tau)^{\varsigma}\sqrt{(\breve{f}\,'(0))^2 + ((\breve{g}'(0))^2)^{\frac{1}{2}}} \quad \text{.....(21)}$$

The local Nusselt number for the concerned flow problem is

$$Nu_{\breve{z}} = \left(\frac{R_0 q_{\breve{w}}}{k(T_{\breve{w}} - T_\infty)}\right)_{\breve{z}=0} \quad \text{.....(22)}$$

$$Nu_{\breve{z}}(Re)^{\frac{n-1}{n+1}} = -(1+\tau)(1+R)\theta'(0) \qquad q_{\breve{w}} = -k\left(\frac{\partial T}{\partial\breve{r}}\right)\Big|_{\breve{z}=0} + (q_{\breve{r}})_{\breve{w}} \quad \text{.....(23)}$$

Here, $Re^{\frac{1}{2}} = \left(\frac{\Omega R_0^2\rho}{\mu}\right)^{\frac{1}{2}}$

Material and Methods

Analytical solution. The homotopy analysis method (HAM) is a sturdy and effective approach for the solution of fluid mechanics problems. HAM is a semi-analytical approach to solve nonlinear PDEs/ODE's. The HAM employs the idea of the homotopy from topology to generate a convergent collection answer for nonlinear structures. This is enabled by way of using a homotopy Maclaurin series to deal with the nonlinearities in the system. Therefore, HAM is a semi analytical technique.

Here, the Zeroth-order based deformation with initial approximations $\breve{h}_0$, $\breve{f}_0$, $\breve{g}_0$, θ_0 and operators $L_{\breve{h}}$, $L_{\breve{f}}$, $L_{\breve{g}}$ and L_θ are considered as

$$\theta_0 = e^{-\xi},\ \breve{g}_0 = e^{-\xi},\ \breve{h}_0 = 0,\ \breve{f}_0 = Ae^{-\xi} \quad \text{.....(24)}$$

$$L_\theta = -\theta + \theta'',\ L_{\breve{g}} = -\breve{g} + \breve{g}'',\ L_{\breve{h}} = \breve{h}',\ L_{\breve{f}} = -\breve{f} + \breve{f}'''\ \text{...(25)}$$

and

$$L_{\breve{h}}[C1] = 0,\ L_{\breve{f}}[C_2e^{\xi} + C_3e^{-\xi}] = 0,\ L_{\breve{g}}[C_4e^{\xi} + C_5e^{-\xi}] = 0,\ L_\theta[C_6e^{\xi} + C_7e^{-\xi}] = 0 \quad \text{.....(26)}$$

in which C_b (b=1–7) are elaborated constants. Let us consider $p \in [0,1]$ specifying the settling parameters, then the zeroth-order deformation problem can take the form

$$(1-p)L_{\breve{h}}[\breve{H}(\breve{\xi};p) - \breve{h}_0(\breve{\xi})] = p\hbar_{\breve{h}}N_{\breve{h}}[\breve{H}(\breve{\xi};p), \breve{F}(\breve{\xi};p)],\ (1-p)L_{\breve{f}}[\breve{F}(\breve{\xi};p) - \breve{f}_0(\breve{\xi})] = p\hbar_{\breve{f}}N_{\breve{f}}[\breve{F}(\breve{\xi};p), \breve{H}(\breve{\xi};p), \breve{G}(\breve{\xi};p)],$$

$$(1-p)L_{\breve{g}}[\breve{G}(\breve{\xi};p) - \breve{g}_0(\breve{\xi})] = p\hbar_{\breve{g}}N_{\breve{g}}[\breve{G}(\breve{\xi};p), \breve{H}(\breve{\xi};p), \breve{F}(\breve{\xi};p)],\ (1-p)L_\theta[\vartheta(\breve{\xi};p) - \theta_0(\breve{\xi})] = p\hbar_\theta N_\theta[\vartheta(\breve{\xi};p), F(\breve{\xi};p), G(\breve{\xi};p)] \quad \text{.....(27)}$$

Here, the nonzero auxiliary parameter are represented by $\hbar_\theta$, $\hbar_{\breve{g}}$, $\hbar_{\breve{f}}$ and $\hbar_{\breve{h}}$ nonlinear operators can be N_θ, $N_{\breve{g}}$, $N_{\breve{f}}$ and $N_{\breve{h}}$

$$N_{\breve{h}}[\breve{H}(\breve{\xi};p), \breve{F}(\breve{\xi};p)] = 2\breve{F} + \frac{\partial \breve{H}}{\partial \breve{\xi}} + \breve{\xi}\grave{o}\breve{\zeta}\frac{\partial \breve{H}}{\partial \breve{\xi}} \quad \text{.....(28)}$$

$$N_{\breve{f}}[\breve{F}(\breve{\xi};p), \breve{G}(\breve{\xi};p), \breve{H}(\breve{\xi};p)] = (1+\tau)^{2\zeta}(Re)^{\frac{1-n}{1+n}}\frac{\partial^2 \breve{F}}{\partial \breve{\xi}^2} - \breve{F}^2 + \breve{G}^2 - \breve{\xi}\grave{o}\breve{\zeta}\breve{F}\frac{\partial \breve{F}}{\partial \breve{\xi}} - \breve{H}\frac{\partial \breve{F}}{\partial \breve{\xi}} - M\breve{F} - \beta\breve{F} + Gr\partial \quad \text{.....(29)}$$

$$N_{\breve{g}}[\breve{G}(\breve{\xi};p), \breve{F}(\breve{\xi};p), \breve{H}(\breve{\xi};p)] = (Re)^{\frac{1-n}{1+n}}(1+\tau)^{2\zeta}\frac{\partial^2 \breve{G}}{\partial \breve{\xi}^2} - 2\breve{F}\breve{G} - \breve{\xi}\grave{o}\breve{\zeta}\breve{F}\frac{\partial \breve{G}}{\partial \breve{\xi}} - \breve{H}\frac{\partial \breve{G}}{\partial \breve{\xi}} - M\breve{G} - \beta\breve{G} \quad \text{.....(30)}$$

$$N_\theta[\vartheta(\breve{\xi};p), \breve{F}(\breve{\xi};p), \breve{H}(\breve{\xi};p)] = \frac{1}{Pr}(1+R)(Re)^{\frac{1-n}{1+n}}\frac{\partial^2 \vartheta}{\partial \breve{\xi}^2} + M\psi\breve{F}^2 + M\psi\breve{G}^2 - \breve{\xi}\grave{o}\breve{\zeta}\breve{F}\frac{\partial \vartheta}{\partial \breve{\xi}} - \breve{H}\frac{\partial \vartheta}{\partial \breve{\xi}} \quad \text{.....(31)}$$

The m[th] order deformation problems can be presented as:

$$L_{\breve{h}}[\breve{h}_m(\breve{\xi}) - \chi_m\breve{h}_{m-1}(\breve{\xi})] = \hbar_{\breve{h}}R_{\breve{h},m}(\breve{\xi}),$$
$$L_{\breve{f}}[\breve{f}_m(\breve{\xi}) - \chi_m\breve{f}_{m-1}(\breve{\xi})] = \hbar_{\breve{f}}R_{\breve{f},m}(\breve{\xi}),$$
$$L_{\breve{g}}[\breve{g}_m(\breve{\xi}) - \chi_m\breve{g}_{m-1}(\breve{\xi})] = \hbar_{\breve{g}}R_{\breve{g},m}(\breve{\xi}),$$
$$L_\theta[\theta_m(\breve{\xi}) - \chi_m\theta_{m-1}(\breve{\xi})] = \hbar_\theta R_{\theta,m}(\breve{\xi}) \quad \text{.....(32)}$$

$$\breve{h}_m(0) = 0,\ \breve{f}_m(0) = A,\ \breve{f}_m(\infty) = 0,\ \breve{g}_m(0) = 1,\ \breve{g}_m(\infty) = 0,\ \theta_m(0) = 1,\ \theta_m(\infty) = 0 \quad \text{.....(33)}$$

Here, $R_{\breve{h},m}$, $R_{\breve{f},m}$, $R_{\breve{g},m}$ and $R_{\theta,m}$ can be written as:

$$R_{\breve{h},m}(\xi) = 2\breve{f}_{m-1} + \breve{h}_{m-1} + \xi\grave{o}\breve{\zeta}\breve{f}_{m-1} \quad \text{.....(34)}$$

$$R_{\breve{f},m}(\xi) = (Re)^{\frac{1-n}{1+n}}(1+\tau)^{2\zeta}\breve{f}''_{m-1} - \breve{f}^2_{m-1} - \breve{g}^2_{m-1} - \xi\grave{o}\breve{\zeta}\sum_{k=0}^{m-1}\breve{f}'_k\breve{f}_{m-1-k} - \sum_{k=0}^{m-1}\breve{f}'_k\breve{h}_{m-1-k} - M\breve{f}_{m-1} - \beta\breve{f}_{m-1} + Gr\theta_{m-1} \quad \text{.....(35)}$$

$$R_{\breve{g},m}(\xi) = (Re)^{\frac{1-n}{1+n}}(1+\tau)^{2\zeta}\breve{g}''_{m-1} - 2\sum_{k=0}^{m-1}\breve{g}_k\breve{f}_{m-1-k} - \xi\grave{o}\breve{\zeta}\sum_{k=0}^{m-1}\breve{g}'_{m-1}\breve{f}_{m-1-k} - \sum_{k=0}^{m-1}\breve{g}'_k\breve{h}_{m-1-k} - M\breve{g}_{m-1} - \beta\breve{g}_{m-1} \quad \text{.....(36)}$$

$$R_{\theta,m}(\xi) = \frac{1}{Pr}(1+R)(Re)^{\frac{1-n}{1+n}}\theta''_{m-1} + M\psi\breve{f}^2_{m-1} + M\psi\breve{g}^2_{m-1} - \xi\grave{o}\breve{\zeta}\sum_{k=0}^{m-1}\theta'_k\breve{f}_{m-1-k} - \sum_{k=0}^{m-1}\theta_k\breve{h}_{m-1-k} \quad \text{.....(37)}$$

$$\chi_m = \begin{cases} 0, & m \le 1 \\ 1, & m \ge 1 \end{cases} \quad \text{.....(38)}$$

The ordinary solutions ($\breve{h}_m$, $\breve{f}_m$, $\breve{g}_m$ and θ_m) containing the distinct solutions ($\breve{h}^*_m$, $\breve{f}^*_m$, $\breve{g}^*_m$ and θ^*_m) can be followed as:

$$\breve{h}_m(\xi) = \breve{h}^*_m(\xi) + C_1,$$

$$\breve{f}_m(\xi) = \breve{f}^*_m(\xi) + C_2 e^{\xi} - C_3 e^{-\xi},$$

$$\breve{g}_m(\xi) = \breve{g}^*_m(\xi) + C_4 e^{\xi} - C_5 e^{-\xi},$$

$$\theta_m(\xi) = \theta^*_m(\xi) + C_6 e^{\xi} - C_7 e^{-\xi} \quad \text{.....(39)}$$

Convergence analysis. HAM series solution is dependent on auxiliary parameters by $\hbar_{\breve{f}}$ and $\hbar_\theta$. The convergence of series solutions is achieved at 8^{th} order of approximation. The convergence region of these auxiliary parameters are $-1.1 \le \hbar_{\breve{f}} \le -0.5$ and $-0.9 \le \hbar_\theta \le -0.1$. The solution converge in ξ $(0 \le \xi \le \infty)$ when ò=0.3, ζ=0.1, n=1, τ =1, Gr=0.9, β=0.6, M=0.7, Re=0.9, R=0.7, ψ =0.1, Pr=1.5, A=0.3, $\hbar_h$ = –0.5, $\hbar_h$=-0.5, $\hbar_f$ = –0.5, $\hbar_g$ = –0.5 and $\hbar_\theta$ = –0.1. Further, convergence rate of HAM solutions for different parameters can be seen in Table 1.

Results and Discussion

Here, the discussion made on the consequences of diverse embedded fluid parameters *via* Nusselt number, skin friction coefficient, temperature and velocity profiles.

Radial and axial velocities analysis. Figures 3-7 shows the behaviors of axial and radial velocity profiles. Figure 3 presented the influence of Hartmann number M on the fluid motion. It is noticed that for the larger values of Hartmann number M, there is a significant decrease in velocity profile, while opposite behaviour can be seen for axial velocity $\breve{h}'(\xi)$. Figure 4 depicted the increased amount of Lorentz force for a larger value of Hartmann number M, which helps to produce the resistance in solid particles. Therefore, both velocity components are decreased. Figure 5 illustrates the significance of stretching number A on the velocity distribution. It is observed that for higher A the magnitude of $\breve{h}(\xi)$ reduces. Figures 6-7 represented the axial and radial velocity profiles for power-law index ζ in terms of larger disk thickness. The upward trend is for axial velocity distribution whereas, the downward trend is for radial velocity profile in terms of a higher amount of ζ.

Table 1. Convergence rate ζ=0.1, τ=1, Gr=0.3, β=0.7, M=0.7, R=0.7, ψ=0.1, Pr=1.7.

Order of approximation	$h''(0)$	$-f'(0)$	$-g'(0)$	$-\theta'(0)$
1.0	0.6150	0.0087	1.3240	0.6992
3.0	0.0412	0.0348	1.3701	0.5219
6.0	0.0367	0.0183	1.3659	0.4477
9.0	0.0344	0.0158	1.3635	0.4284
15.0	0.0314	0.0153	1.3633	0.4212
17.0	0.0313	0.0152	1.3634	0.4211
20.0	0.0313	0.0153	1.3634	0.4212
30.0	0.0313	0.0153	1.3634	0.4212
35.0	0.0313	0.0153	1.3634	0.4212
40.0	0.0313	0.0153	1.3634	0.4212

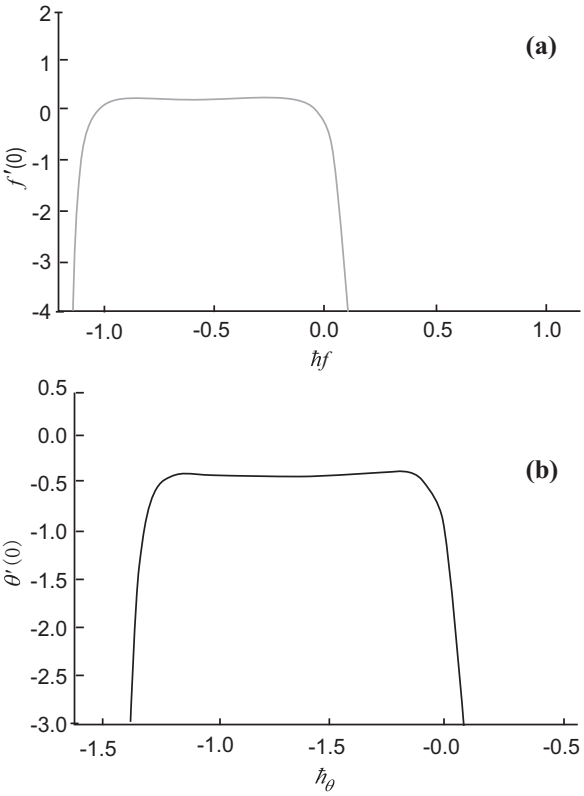

Fig. 2a&b. h-curves of auxiliary parameters $\hbar_f$ and $\hbar_\theta$.

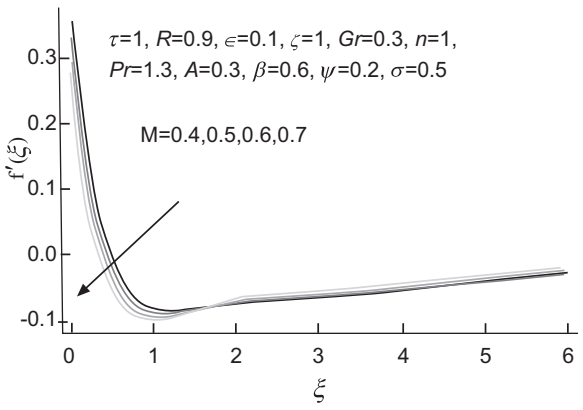

Fig. 3. Significance of M on $f'(\xi)$.

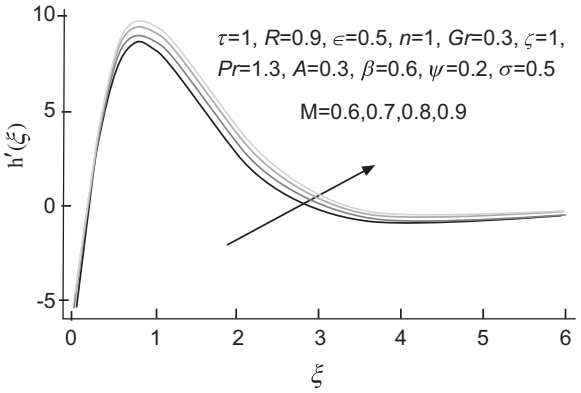

Fig. 4. Significance of M on $h'(\xi)$.

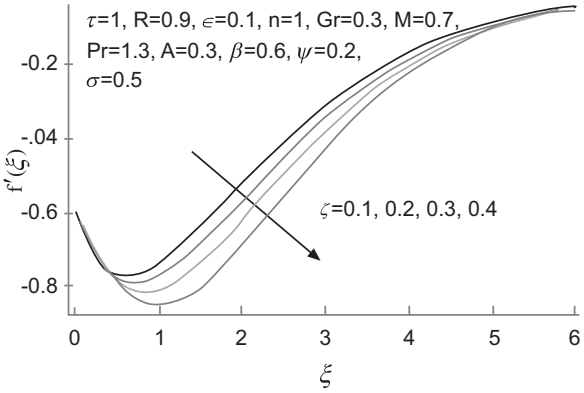

Fig. 7. Significance of ζ on $f'(\xi)$.

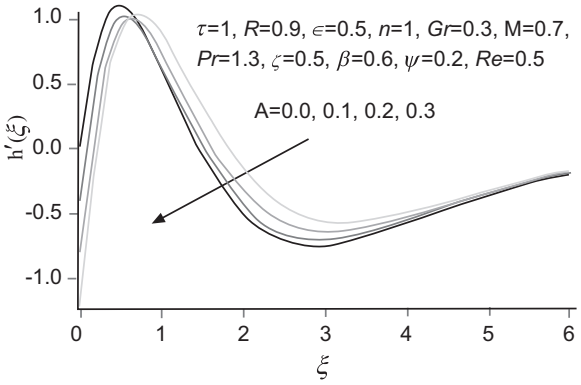

Fig. 5. Significance of A on $h'(\xi)$.

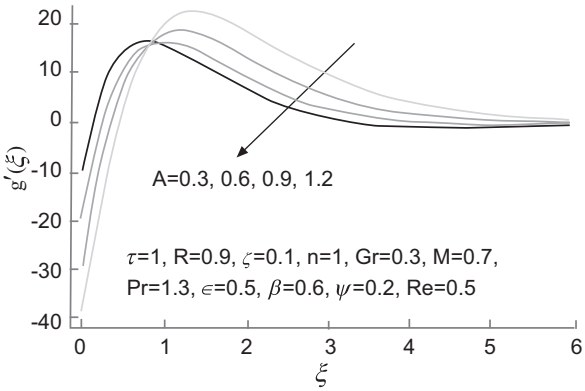

Fig. 8. Significance of A on $g'(\xi)$.

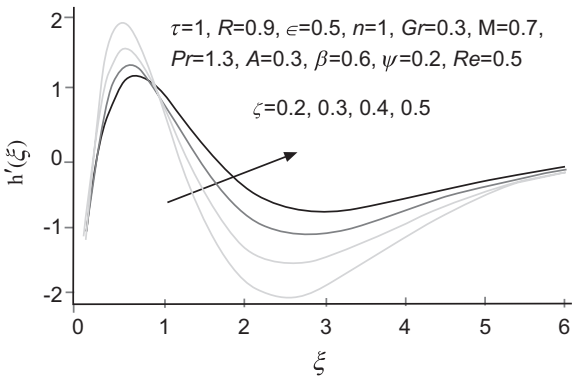

Fig. 6. Significance of ζ on $h'(\xi)$.

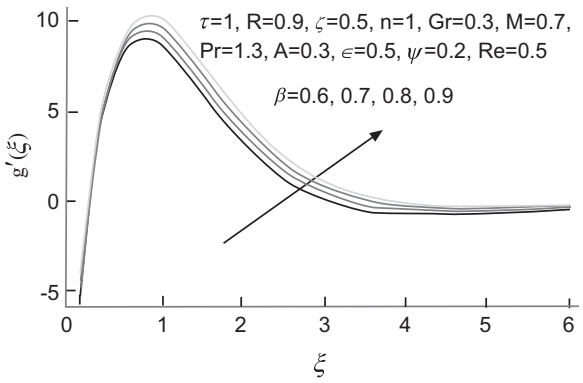

Fig. 9. Significance of β on $g'(\xi)$.

Tangential velocity analysis. Figures 8 and 9 display that for increasing values of both stretching parameter A and Hartmann number β the tangential velocity $\breve{g}'(\xi)$ shows opposite trend. Figure 10 described the impact of Hartmann number M on tangential velocity $\breve{g}'(\xi)$. For increasing the value of Hartmann number M tangential velocity profile $\breve{g}'(\xi)$ enhances because of resistance which is produced by the Lorentz forces. Figure 11 shows the effect of the disk thickness by power-law index ζ on the tangential velocity profile

$\bar{g}'(\xi)$. As a result, tangential velocity increases due to the increasing value of the power-law index ζ.

Temperature analysis. Figure 12 represents the effect of stretching parameter A on the temperature field. The increasing value in A, temperature $\theta'(\xi)$ decreases but rotational velocity reduces. This is due to less resistance, which is produced between the particles therefore temperature decreases. Figure 13 shows the behavior of radiation parameter R on $\theta'(\xi)$. Here the temperature profile $\theta'(\xi)$ enlarges when radiation behaves powerful. The mean absorption coefficient reduces due to increasing radiation parameter R. Hence the ratio between radiative heat transfer and fluid is enhanced. The impact of disk thickness by ζ on the temperature field is displayed in Fig. 14. Increased in ζ, the temperature profile enhanced.

Skin friction coefficient. Figures 15-16 the behaviour of thickness of the disk by the exponent ζ opposite to stretching parameter A. It is concluded that the skin

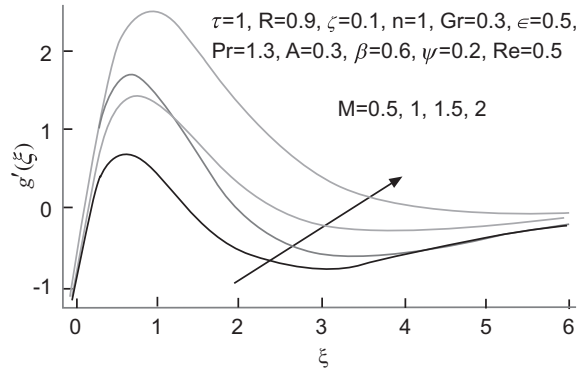

Fig. 10. Significance of M on $g'(\xi)$.

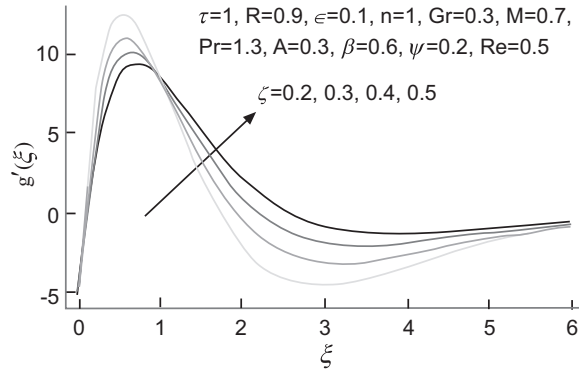

Fig. 11. Significance of ζ on $g'(\xi)$.

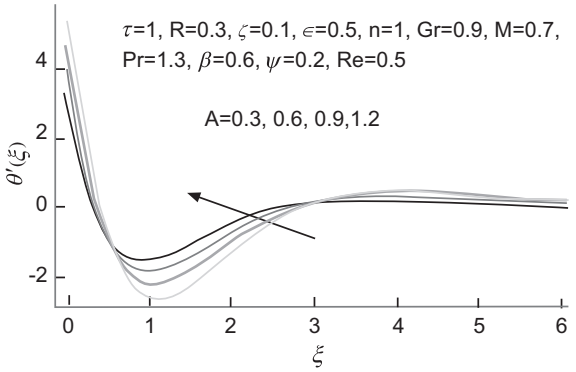

Fig. 12. Significance of A on $\theta'(\xi)$.

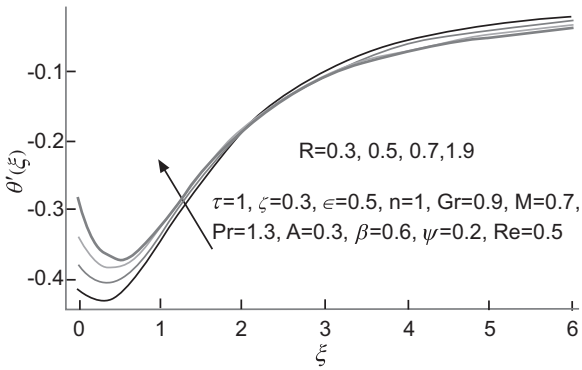

Fig. 13. Significance of R on $\theta'(\xi)$.

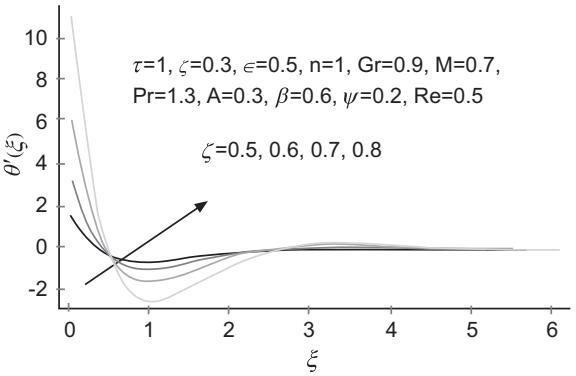

Fig. 14. Significance of ζ on $\theta'(\xi)$.

friction reduces when ζ is increased. On the other hand, it is enhanced for the larger Grashoff number Gr.

Nusselt number. Figures 17-18 show the effect of disk thickness by utilizing the power-law index ζ and radiation parameter R on the Nusselt number. Rate of

heat transfer shows uplift performance for higher R and opposite for thickness of disk by ζ.

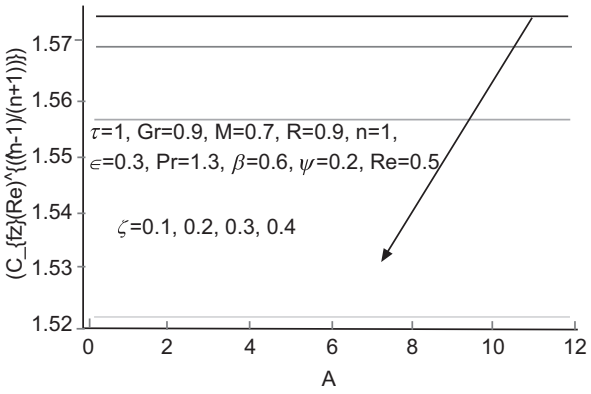

Fig. 15. Influence of ζ on $C_{fz}(Re)^{\frac{n-1}{n+1}}$.

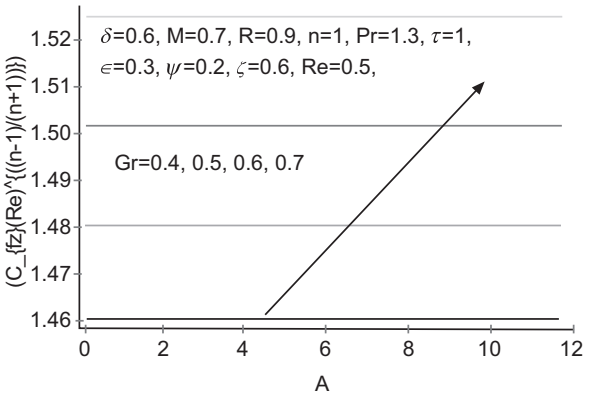

Fig. 16. Significance of Gr on $C_{fz}(Re)^{\frac{n-1}{n+1}}$.

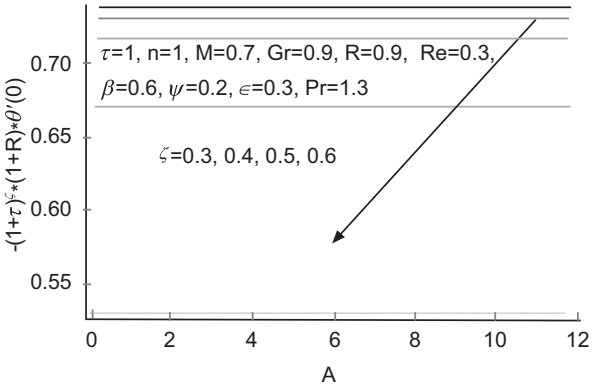

Fig. 17. Significance of ζ on $Nu(\mathrm{Re})^{0.5}$.

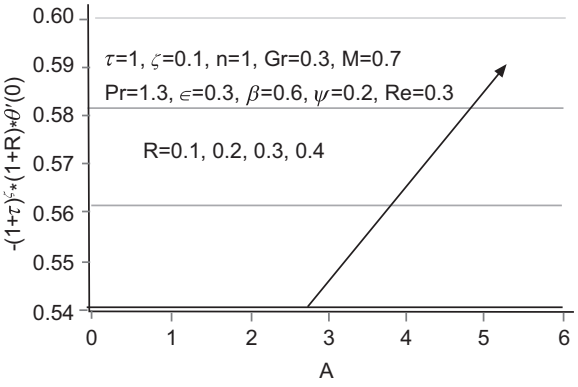

Fig. 18. Significance of R on $Nu(\mathrm{Re})^{0.5}$.

Conclusions

A mathematical model and an analytical solution has been explored for the mixed convective flow of ferrofluid with variable thickness in rotating porous disk in the presence of radiation and magnetic effects. Utilizing appropriate scaling transformations, a system of coupled non-linear PDEs are converted to ODEs.

- Tangential velocity profile decreases for larger Hartmann number M.
- With an increase in values of stretching number A, radiation parameter R and power-law index ζ temperature of fluid shows upward trend.
- For larger values of disk thickness power-law index ζ, tangential velocity, axial, radial velocities and temperature field enhance in each case.
- Skin friction increases by increasing the values of Grashoff number Gr, while decreasing for the power-law index ζ.
- Nusselt number decreases for the higher amount of power-law index ζ and radiation parameter R.

Recommendations

It is an amazing scope to deal and continue with this interesting research studies. The entire body of this work is packed with modeling and simulation for the heat transportation mechanism in ferrofluid through a porous surface with variable thickness in diverse directions. Certainly, a bundle of work is still final associated with this work. In this have a look at, one problem is considered, however not all, similarly extensions are feasible. Firstly, to take advantage, the extra information about the enhancement of heat transfer, a few other suitable models can be applied. Additionally, the overall performance of some different kind of fluid,

shapes and ideal materials ought to be investigated through taking inside the numerous styles of surfaces. Secondly, the ferrofluid version towards porous stretching disk may be applied with different chemical reactions. Although, this is a quarter of in addition evaluation that needs to be confirmed in the way to upgrade our expertise of ferrofluid flow inside the subject line to time structured flows. Therefore, to acknowledge heat transfer efficiently, the information applied in this work is not for the experimental fashions, however simplest utilized for the convergence of issues. Consequently, to do the comparative evaluation of our theoretical examination, there's nonetheless motivation require for the exact experimental effects of the existing work. In addition, applications of the proposed type of flow can be seen in fields like medicines, electronics engineering, mechanical engineering, spacecraft propulsion and in Material Science.

Conflict of Interest. The authors declare that they have no conflict of interest.

References

Agarwal, R., Chakraborty, S. 2022. Analytics with blood on hybrid paper-rotating disc device. *Sensors and Actuators Reports*, **4:** DOI: 10.1015/j.snr.2022.100122.

Algehyne, E.A., Alrihieli, H.F., Saeed, A., Alduais, F.S., Hayat, A.U., Kumam, P. 2022. Numerical simulation of 3D Darcy-Forchheimer fluid flow with the energy and mass transfer over an irregular permeable surface. *Scientific Reports*, **12:** 1-14.

Bhandari, A. 2020. Study of ferrofluid flow in a rotating system through mathematical modeling. *Mathematics and Computers in Simulation*, **178:** 290-306.

Dhibi, B., Ben-Beya, B. 2021. Three-dimensional numerical simulation of ferrofluid magneto-convection in cubical enclosure heated with an inner spherical hot block. *International Journal of Modern Physics C*, **32:** 1-23.

Gul, T., Ullah, M.Z., Alzahrani, A.K., Zaheer, Z., Amiri, I.S. 2020. MHD thin film flow of kerosene oil based CNTs nano fluid under the influence of Marangoni convection. *Physica Scripta*, **95:** DOI: 10.1088/1402-4896/ab47C4

Gul, T., Bilal, M., Shuaib, M., Mukhtar, S., Thounthong, P. 2020. Thin film flow of the water-based carbon nanotubes hybrid nanofluid under the magnetic effects. *Heat Transfer*, **49:** 3211-3227.

Gul, T., Gul, R.S., Noman, W., Hussain, F., Amiri, I.S. 2020. Controlling of the melting through porous medium and magnetic field. *Measurement and Control*. DOI: 10.1177/0020294020919918.

Huang, X., Zhang, X., Wang, Y. 2021. Numerical simulation of Ferrofluid lubricated rough elliptical contact with start-up motion. *Applied Mathematical Modelling*, **91:** 232-260.

Haq, S.U., Khan, M.A., Khan, Z.A., Ali, F. 2020. MHD effects on the channel flow of a fractional viscous fluid through a porous medium: an application of the Caputo-Fabrizio time-fractional derivative. *Chinese Journal of Physics*, **65:** 14-23.

Khan, M.I., Qayyum, S., Shah, F., Kumar, R.N., Gowda, R.P., Prasannakumara, B.C., Kadry, S. 2021. Marangoni convective flow of hybrid nanofluid ($MnZnFe_2O_4$-$NiZnFe_2O_4$-H_2O) with Darcy Forchheimer medium. *Ain Shams Engineering Journal*, **12:** 3931-3938.

Mongia, C., Goyal, D., Sehgal, S. 2022. Vibration response-based condition monitoring and fault diagnosis of rotary machinery. *Materials Today: Proceedings*, **50:** 679-683.

Prusty, K.K., Sahoo, S.N., Mishra, S.R. 2021. Exploration of heat transfer effect in a magneto hydrodynamics flow of a micro polar fluid between a porous and a nonporous disk. *Heat Transfer*, **50:** 1042-1055.

Sharma, K., Kumar, S., Narwal, A., Mebarek-Oudina, F., Animasaun, I.L. 2022. Convective MHD fluid flow over stretchable rotating disks with dufour and Soret effects. *International Journal of Applied and Computational Mathematics*, **8:** 1-12.

Shahzad, F., Jamshed, W., El Din, S.M., Shamshuddin, M., Ibrahim, R.W., Raizah, Z. 2022. Second order convergence analysis for Hall effect and electromagnetic force on ternary nanofluid flowing via rotating disk. *Scientific Reports*, **12:** 1-21.

Shamshuddin, M.D., Akkurt, N., Saeed, A., Kumam, P. 2022. Radiation mechanism on dissipative ternary hybrid nanoliquid flow through rotating disk encountered by Hall currents: HAM solution. *Alexandria Engineering Journal*, **65:** 543-559.

Salawu, S.O., Shamshuddin, M.D., Bég, O.A. 2022. Influence of magnetization, variable viscosity and thermal conductivity on Von Karman swirling flow of H_2O-Fe_3O_4 and H_2O-Mn-$ZnFe_2O_4$ ferromagnetic nanofluids from a spinning DISK: Smart spin coating simulation. *Materials Science and Engineering-B*, **279,** DOI: 10.1016/j.mseb.2022.115659.

Sadeghi, M.S., Tayebi, T., Dogonchi, A.S., Nayak, M.K., Waqas, M. 2021. Analysis of thermal behavior of magnetic buoyancy-driven flow in ferrofluid-filled wavy enclosure furnished with two circular cylinders. *International Communications in Heat and Mass Transfer*, **120:** 104951. DOI: 10.1016/j.icheatmasstransfer.2020.104951

Socoliuc, V., Marin, C.N. 2021. The effect of long time exposure to light of a water-based ferrofluid on its low frequency complex magnetic permeability. *Journal of Magnetism and Magnetic Materials*, **523:** 167635. DOI: 10.1016/j.jmmm.2020.167635

Shamshuddin, M.D., Eid, M.R. 2021. Magnetized nanofluid flow of ferromagnetic nanoparticles from parallel stretchable rotating disk with variable viscosity and thermal conductivity. *Chinese Journal of Physics*, **74:** 20-37.

Saratha, S.R., Krishnan, G.S.S., Bagyalakshmi, M. 2021. Analysis of a fractional epidemic model by fractional generalized homotopy analysis method using modified Riemann-Liouville derivative. *Applied Mathematical Modelling*, **92:** 525-545.

Shamshuddin, M.D., Mishra, S.R., Bég, O.A., Kadir, A. 2019. Numerical study of heat transfers and viscous flow in a dual rotating extendable disk system with a non-Fourier heat flux model. *Heat Transfer Asian Research*, **48:** 435-459.

Zari, I., Ali, F., Khan, T.S., Shafiq, A. 2022. Radiative Hiemenz flow towards a stretching Riga plate in hybrid nanofluid. *International Communications in Heat and Mass Transfer*, **139:** 106492. DOI: 10.1016/j.icheatmasstransfer.2022.106492

Zontul, H., Hamzah, H., Sahin, B. 2021. Impact of periodic magnetic source on natural convection and entropy generation of ferrofluids in a buffed cavity. *International Journal of Numerical Methods for Heat and Fluid Flow*, **31:** 3457-3575.

Zari, I., Shafiq, A., Khan, T.S., Haq, S. 2021. Marangoni convective flow of GO-kerosene-and GO-water-based casson nanoliquid toward a penetrable riga surface. *Brazilian Journal of Physics*, **51:** 1747-1762.